Nanoscale

PAPER

View Article Online
View Journal | View Issue

Cite this: *Nanoscale*, 2020, **12**, 4909

Near full light absorption and full charge collection in 1-micron thick quantum dot photodetector using intercalated graphene monolayer electrodes†

Wenjun Chen, Seungbae Ahn, Marquez Balingit, Jiaying Wang, Malcolm Lockett and Oscar Vazquez-Mena *

Received 20th November 2019,
Accepted 4th February 2020

DOI: 10.1039/c9nr09901h

rsc.li/nanoscale

Quantum dots (QDs) offer several advantages in optoelectronics such as easy solution processing, strong light absorption and size tunable direct bandgap. However, their major limitation is their poor film mobility and short diffusion length (<250 nm). This has restricted the thickness of QD film to ~200–300 nm due to the restriction that the diffusion length imposes on film thickness in order to keep efficient charge collection. Such thin films result in a significant decrease in quantum efficiency for λ > 700 nm in QDs photodetector and photovoltaic devices, causing a reduced photoresponsivity and a poor absorption towards the near-infrared part of the sunlight spectrum. Herein, we demonstrate 1 μm thick QDs photodetectors with intercalated graphene charge collectors that avoid the significant drop of quantum efficiency towards λ > 700 nm observed in most QD optoelectronic devices. The 1 μm thick intercalated QD films ensure strong light absorption while keeping efficient charge extraction with a quantum efficiency of 90%–70% from λ = 600 nm to 950 nm using intercalated graphene layers as charge collectors with interspacing distance of 100 nm. We demonstrate that the effect of graphene on light absorption is minimal. We achieve a time-modulation response of <1 s. We demonstrate that this technology can be implemented on flexible PET substrates, showing 70% of the original performance after 1000 times bending test. This system provides a novel approach towards high-performance photodetection and high conversion photovoltaic efficiency with quantum dots and on flexible substrates.

1. Introduction

Photodetection and photovoltaic devices are of great relevance for a variety of applications, such as optical communications, imaging, sensing and harvesting. Beyond the visible region, the near-infrared (NIR) is especially important in night vision, medicine and other photodetection devices.[1,2] Similarly, a significant part of the sunlight spectrum is in the NIR, contributing with a significant number of photons that for single junction photovoltaic cells give the same contribution as visible photons. Quantum dots (QDs) have emerged as promising materials for photodetection and photovoltaics due to their easy and low cost synthesis and solution processing, and their high-quality optoelectronic properties such as strong light absorption and size tunable direct bandgap.[3,4] However, the short diffusion length in QDs films (L_D < 250 nm) limits their useful thickness to ~200–500 nm;[5–9] this is a result of the well-known compromise between light absorption and diffusion transport charge extraction in QDs films. Visible photons have a penetration depth <200 nm, therefore they are effectively absorbed by ~300 nm thick QD films. However, in the near-infrared range, the penetration depth increases drastically to >400 nm and thin QD films t ~ 200–500 nm cannot capture NIR light efficiently (the penetration depth of PbS QDs is shown in the ESI in Fig. S1†). This results in a significant drop of quantum efficiency (EQE) starting at λ ~ 700 nm that is present in several top performing solar cells reported recently.[6,8–11] This is a consequence of their short L_D limiting the QD film thickness (t < 500 nm). Similarly, QD and hybrid QD/2D photodetectors show a drop in photoresponsivity as light wavelength increases towards the NIR range,[12–14] limiting the performance of QDs optoelectronics in the NIR range.

Herein, we report the use of interacted graphene (Gr) transparent electrodes to achieve 1 micron thick QD films enhan-

Department of NanoEngineering, Center for Memory and Recording Research, Calibaja Center for Resilient Materials and Systems, University of California San Diego, 9500 Gilman Drive, La Jolla, CA 92093, USA. E-mail: oscarvm@eng.ucsd.edu

† Electronic supplementary information (ESI) available: S1: Penetration depth of light in QD films; S2: Time constants in photodetector time response; S3: Photogain and EQE Calculations; S4: Absorption spectra as function of thickness; S5: Dark current traces and noise levels. See DOI: 10.1039/c9nr09901h

cing light absorption in the near-IR while keeping efficient charge collection. Previously, a novel configuration for QD films with intercalated graphene monolayers was reported, showing improved responsivity and charge extraction compared to QD films with bottom Gr collectors.[15] However, these films reached only 200 nm in thickness due to fabrication and carrier collection constrains. First, their interspacing distance between intercalated graphene electrodes was only ~20 nm, which was not optimal to reach films thicker than 200 nm. Second, they only used bottom contacts, limiting the charge collection from top graphene layers. This resulted in poor performance in the near-infrared (λ > 700 nm) despite the intercalated geometry.[15] Herein, we have tuned and optimized the interspacing between graphene layers to 100 nm, and we have implemented vertical interconnect access electrodes (VIAs) to contact each of the intercalated graphene layers to achieve thicker films with efficient charge collection, allowing us to reach an unprecedented 1-micron thick QD film (~5 times thicker than the diffusion length) and significantly improve performance in the near-IR. Furthermore, we report similar 1-micron thick QD films on flexible substrates, which shows this technology can be applied to flexible and wearable technologies. Previous reports used a 2D matrix to improve coupling between quantum dots, however, they reach only 600 nm thick QD film for solar cells with high EQE.[9] However, reviews on QD optoelectronics suggest that ~1-micron thick QD films are required to efficiently absorb sunlight in photovoltaic devices.[16–18]

In this work, we show the increase in light absorption as function of thickness with a very limited effect of the graphene intercalated layers on light absorption. The improved performance of intercalated *vs.* non-intercalated (bottom devices) under time modulated light is also shown. We study how the interspacing distance between graphene layers (D_{Gr}) affects the performance of the devices. Then, we study photoresponsivity and show the superior EQE of 1-micron thick QD devices reaching near 90%–70% EQE from λ = 600 to 950 nm, avoiding the drop in performance at $\lambda \sim$ 700 nm observed in previous reports of QD devices.[6,8,10,11] Finally, we show that the same structure can be implemented on flexible devices showing superior photoresponsivity. To the best of our knowledge, this is the best EQE performance in PbS QDs photodetectors reported, which we attribute to the 1-micron thickness enabled by intercalated Gr layers. The use of intercalated Gr collectors presented here, provides an alternative and complementary route to enhance the performance of QD light absorbing optoelectronic devices.

2. Experimental

2.1 Device fabrication

The hybrid photodetector used monolayer CVD graphene from Graphenea and PbS quantum dots synthesized by existing method[29] (fluorescence λ_{em} at 1050 nm). Chromium/gold (10 nm/100 nm) was evaporated to form the electrodes with device dimension of 1 mm × 1 mm by using a shadow mask on SiO_2/Si (280 nm/500 μm) substrate. Graphene was transferred onto the substrate by poly(methyl methacrylate) (PMMA) supporting wet-transfer.[30,31] PbS QDs film was deposited using spin-coating under ambient atmosphere. For each PbS QDs layer, the QDs solution (55 mg mL^{-1} in toluene) was spin-casted at 2500 rpm for 30 s, then a solid-state ligand exchange was performed by flooding the surface with 0.03 M TBAI in methanol for 30 s before spinning dry at 2500 rpm. For the intercalated with VIAs devices, QDs films were partially etched, then chromium/gold (10 nm/100 nm) were deposited by e-beam evaporator, alternating Gr transfer and QDs spin coating were carried out sequentially afterwards. For the bottom Gr/QD system, QDs film was formed layer-by-layer.

2.2 Optical and electrical measurement

UV-Vis absorption. Absorption spectrum was measured using HITACHI UV-Visible/NIR spectrophotometer model UH4150.

Spectral measurements. Current–voltage data were measured using a Keithley 2400 source meter under a xenon lamp and filters (66485-500HX-R1, USFW-100, Newport) with a monochromator (CS260-RG-3-FH-D, Newport). The light intensity was measured with a standard silicon photodiode power sensor (S120VC, Thorlabs) at the same position of the samples. A pinhole of 1 × 1 mm^2 was used to illuminate only the active area.

Photocurrent-power intensity measurements. Current–voltage data were measured using a Keithley 2400 source meter under a λ = 850 nm laser diode (CPS850, Thorlabs) in ambient. In order to achieve different light intensity, absorptive neutral density filters (NE503A, NE510A, NE520A, NE530A, Thorlabs) were employed. The light intensity was measured using a standard silicon photodiode power sensor (S120VC, Thorlabs). A pinhole of 1 × 1 mm^2 was used to illuminate only the active area.

Time modulation response measurements. A λ = 850 nm laser diode (CPS850, Thorlabs) is time-modulated by a function generator Keysight 33500B Waveform Generator. Current–voltage data were measured in ambient conditions using a Keithley 2400 source meter.

3. Results and discussion

Diagrams illustrating the architecture and operation of bottom and intercalated hybrid Gr/QDs photodetectors are shown in Fig. 1a and b. The intercalated devices are fabricated by sequential and alternating spin coating of PbS QDs with bandgap E_g = 1.18 eV (1050 nm) and wet transfer of graphene monolayers. In Gr/QDs hybrid system, photogenerated holes are transferred to graphene and driven by a bias voltage to produce photocurrent, while photogenerated electrons stay in QDs causing a photogating effect. In the case of bottom devices, only carriers generated within the diffusion length from the bottom contact can be efficiently transferred to graphene, whereas for intercalated layers the carriers can be col-

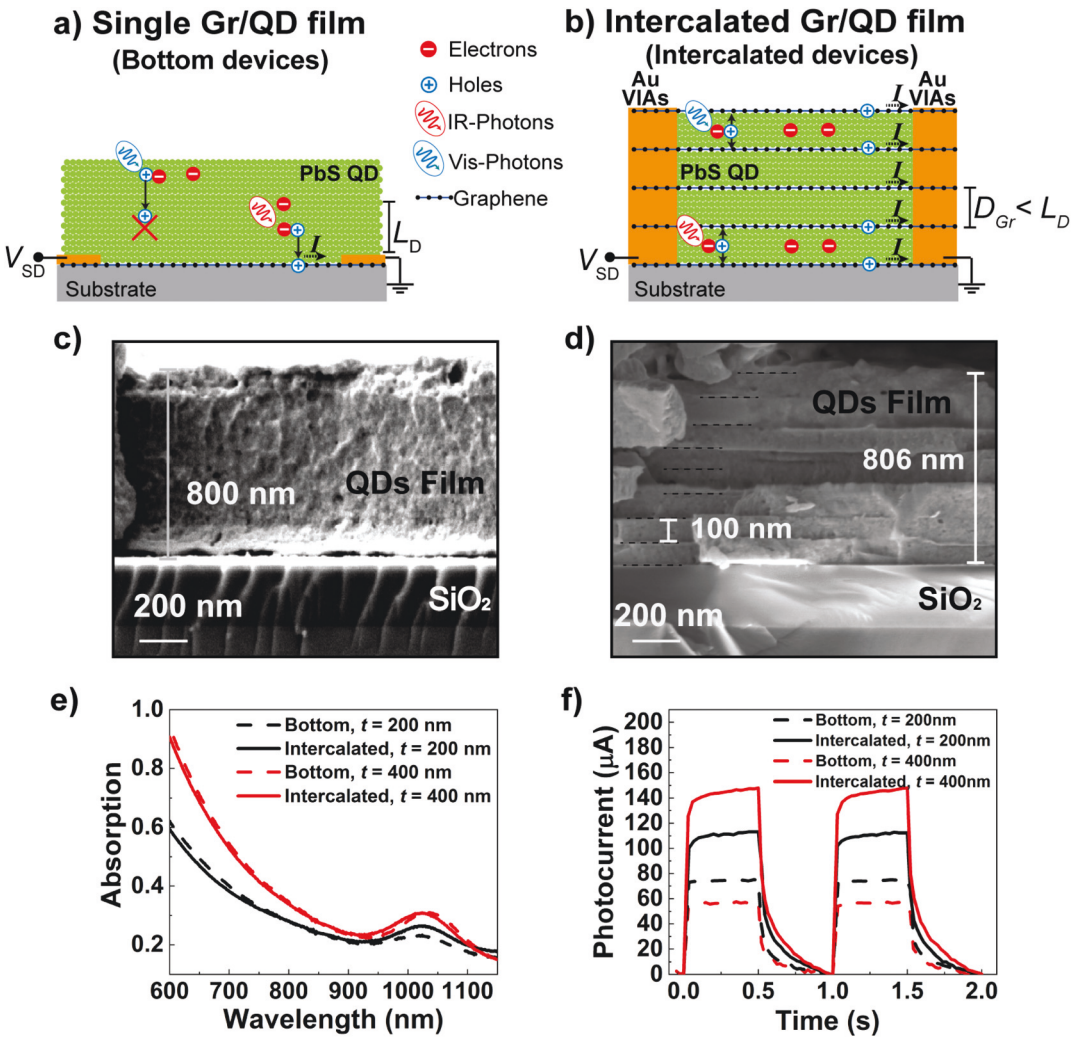

Fig. 1 Bottom and intercalated devices. Schematic images of (a) conventional hybrid Gr/QDs device with single graphene at the bottom (Bottom devices), and (b) intercalated configuration with Au VIAs for enhanced charge collection. SEM images of (c) bottom device and (d) intercalated device both with total QDs film thickness of 800 nm. The layered nature of the intercalated devices is clearly observed. (e) Light absorption spectra of 200 and 400 nm thick devices, showing no significant difference between bottom and intercalated devices. (f) Photocurrent response of 200 and 400 nm thick devices, showing stronger response of intercalated over bottom devices. Measurements were performed using laser excitation at λ = 850 nm and V_{DS} = 1 V.

lected at any point in the film as long as $L_D > D_{Gr}$.[12,19] Fig. 1c and d show SEM cross section images of bottom and intercalated devices 800 nm thick. The intercalated devices have a graphene interspacing of D_{Gr} = 100 nm, with a clear layered structure. Fig. 1e shows the light absorption spectra of QD films with thickness t = 200 and 400 nm with bottom and intercalated graphene layers showing the characteristic exciton absorption peak at $\lambda \sim 1050$ nm. Evidently, thicker films have stronger absorption, but more importantly, the intercalated and bottom devices show similar absorption spectra, indicating that the graphene intercalated layers do not have a significant or degrading effect on the QD absorption. In contrast, intercalated devices have a much higher photoresponse than bottom devices, as shown in the time photoresponse under λ = 850 nm illumination in Fig. 1f. The improvement in photoresponse is more pronounced for the 400 nm than for the 200 nm thick device. The photocurrent of intercalated devices are 112 μA (t = 200 nm) and 148 μA (t = 400 nm), while for the bottom devices are 75 μA (t = 200 nm) and 57 μA (t = 400 nm), indicating that intercalated graphene layers improve photoresponse by enhancing the charge collection.

A critical parameter in intercalated devices is the graphene interspacing (D_{Gr}), which should be smaller than the diffusion length L_D to keep efficient charge collection. At the same time, D_{Gr} should not be so small to the point of making the fabrication process extremely long by requiring too many graphene transfers. The first reported intercalated devices had D_{Gr} = 20 nm,[15] which would require an impractical number of 50 intercalated layers for a 1-micron thick layer. In order to study the effect D_{Gr}, we fabricated 800 nm thick intercalated devices

with varying spacings of D_{Gr} = 100, 133, 166, and 200 nm, which means 9, 7, 6, and 5 graphene layers, respectively, where the number of layers is $\#L = t/D_{Gr} + 1$. Fig. 2a shows the absorption spectroscopy of the t = 800 nm films with different D_{Gr} showing no significant differences. The limited effect of Gr on the absorption of intercalated films has been reported in intercalated QD/Gr devices and is attributed to the low 2% absorption of graphene.[15,20] However, the photoresponsivity does show significant changes with D_{Gr} as shown in Fig. 2b and c. The intercalated device with D_{Gr} = 100 nm gives the best photocurrent ($I_{ph} = I_{light} - I_{dark}$) with lower response for larger D_{Gr}. It is possible that D_{Gr} < 100 nm can give higher responsivity, however, the number of graphene layers required would make it impractical. From these results, we fix D_{Gr} = 100 nm to build intercalated films up to 1-micron in thickness. The time response of the devices shows a fast and slow component as shown in ESI in Fig. S2† and observed previously in first Gr/QD hybrid devices.[12] The fast components is ~70 ms, allowing for sub-second light modulation shown in Fig. 2b. We do not observe major variations in time response for different D_{Gr}. The slow component of the time response is ~3 seconds, which is responsible for the large photogain of the devices analyzed in ESI in Panel S3.† This long lifetime is probably associated to traps in the QDs and causes a long stabilization of the signal, which is more pronounced in the intercalated than bottom devices.

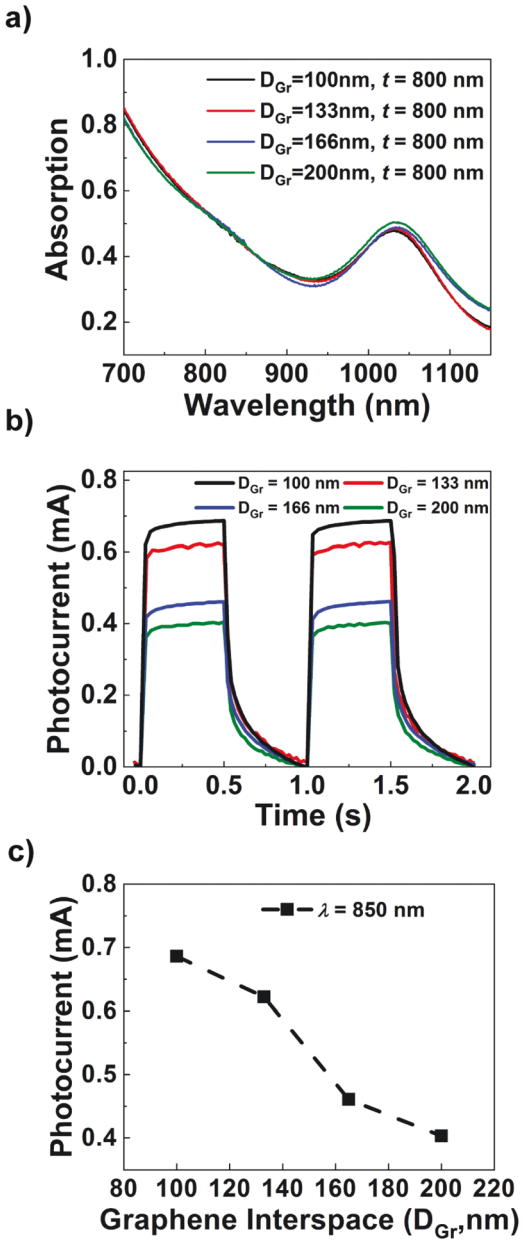

Fig. 2 Effect of graphene interspacing (D_{Gr}) in intercalated devices. (a) Absorption of intercalated QD films with D_{Gr} = 100 nm, 133 nm, 166 nm, and 200 nm and total thickness t = 800 nm. The effect of graphene is limited on light absorption. (b) Light ON/OFF response for intercalated devices with different D_{Gr} and total thickness of t = 800 nm. D_{Gr} = 100 nm gives the best light response with charge extraction decreasing for D_{Gr} > 100 nm. (c) Plot of photocurrent as function of D_{Gr}. Measurements were performed using laser excitation at λ = 850 nm and V_{DS} = 1 V.

Fig. 3a and b show the spectral photoresponsivity ($R = I_{ph}/P_{inc}$, $I_{ph} = I_{Light} - I_{Dark}$) of bottom and intercalated (D_{Gr} = 100 nm) devices with t = 100, 200, 400 and 1000 nm. Fig. 3a shows that for bottom devices, t = 200 nm shows the best performance, keeping efficient charge collection. Thicker t = 400 nm and 1 μm thick bottom devices give lower responsivity. However, it is worth pointing out that the 1 μm thick film shows better performance than t = 100 and 400 nm in the λ = 900–1100 nm, probably due to the infrared photons being absorbed deeper and near to the bottom Gr/QD interface. The intercalated devices in Fig. 3b show a drastic improvement over their corresponding bottom devices. Furthermore, R increases as the thickness increases from 100 nm to 1 μm across the entire spectrum, indicating efficient charge collection as thickness increases. It is also important to point out that for t = 100, 200 and 400 nm intercalated devices, R increases up to $\lambda \sim 700$ nm, but then R decreases as longer wavelengths have deeper penetration depths. In contrast, the 1-micron thick device shows a clear increase in responsivity up to $\lambda \sim 900$ nm. Since the penetration depth for $\lambda \sim 900$ nm is >500 nm, reaching a 1-micron thickness enables to enhance the performance beyond visible range keeping efficient charge collection with intercalated graphene layers. This behavior marks an important contrast with previous hybrid PbS/Gr and PbS/MoS_2 devices with bottom 2D material, which show a clear decrease in responsivity from λ = 600 nm towards λ = 1000 nm.[12,14,21,22] The light absorption spectrum of the intercalated films is shown in ESI in Fig. S4,† showing the clear increase in absorption as the thickness increases. The quantum efficiency can be extracted by estimating the photogain[23] as shown in the ESI in Panel S3.† Using L = 1 mm, $\mu_h \sim$ 400 $cm^2\ V^{-1}\ s^{-1}$, V_{DS} = 10 mV and $\tau_{lifetime}$ = 3.1 s, we obtain a photogain of G = 1.2 × 10^3. The QE is obtained from $R = (QE)G\left(\frac{q\lambda}{hc}\right)$ and is plotted in Fig. 3c, reflecting the improved charge collection as thickness increases beyond the diffusion length ($L_D \sim$ 100–200 nm), breaking its restriction on the film

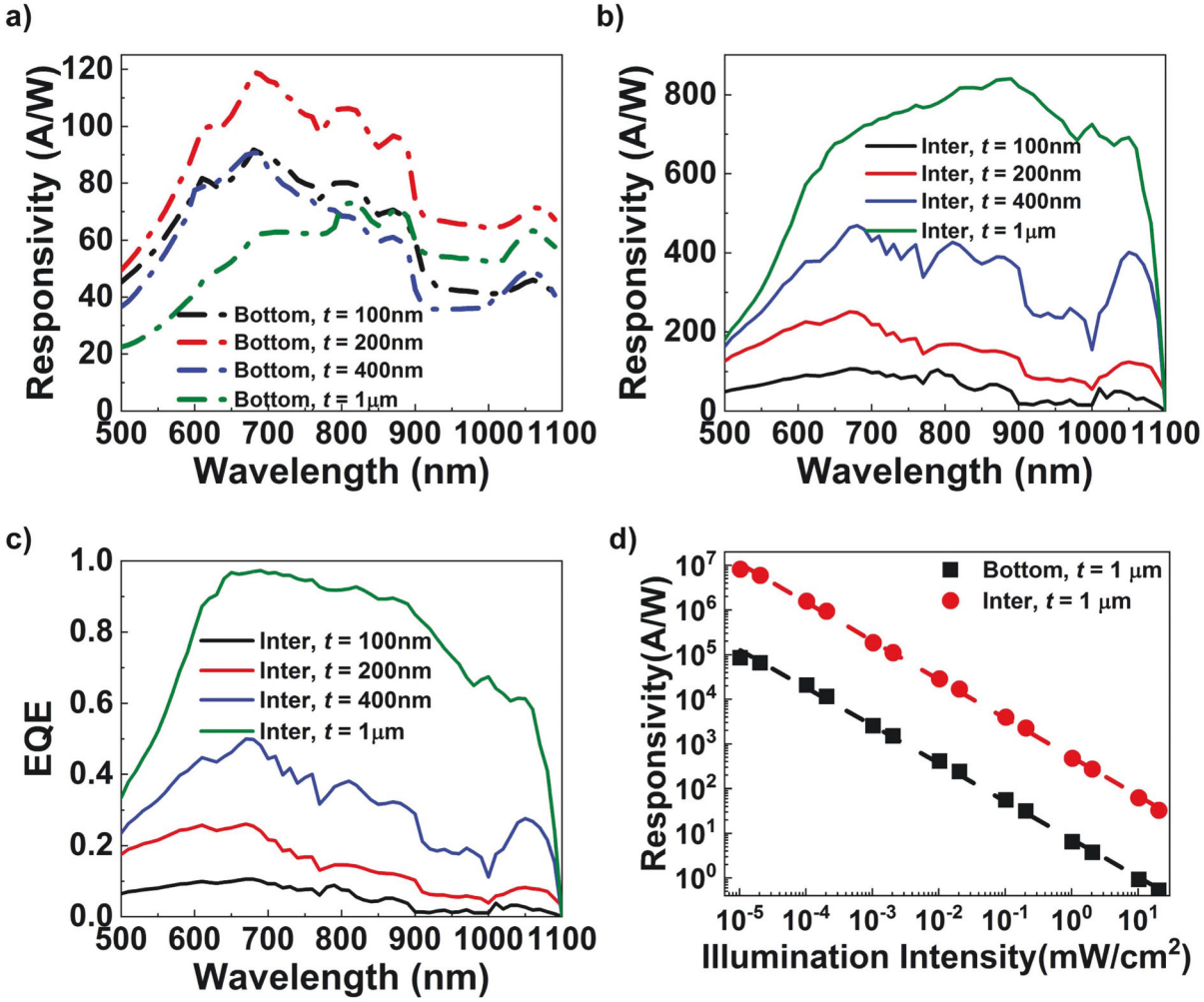

Fig. 3 Spectral response. (a) Spectral responsivity ($R = I_{ph}/P_{inc}$) for bottom devices with different thickness under 10 mV bias. Highest R is obtained at t = 200 nm, which ensures efficient charge collection. (b) Responsivity for intercalated devices, showing that R increases as thickness increases from 100 nm to 1 mm over the entire spectrum. Only the 1-micron thick device keeps R increasing in the $\lambda \sim 600$–900 nm range. (Bias voltage = 10 mV). (c) EQE increases across spectrum for intercalated devices as t increases extracted from Responsivity in (b). Whereas t = 100–400 nm devices show a drop in EQE at λ = 700 nm, the 1 μm thick device keeps EQE without significant drop from 600 nm to 900 nm. (d) R increases as light intensity decreases. Intercalated device shows two orders of magnitude higher R than bottom device. Devices in (d) are under V_{SD} = 5 V and 850 nm laser excitation.

thickness. The QE of the 1μm thick device keeps at 70%–90% from λ = 600 nm to 950 nm, avoiding the drastic drop at λ = 700 nm. Up to our knowledge, this is the first report with a PbS-QD optoelectronic devices having such high EQE avoiding the drop of performance near $\lambda \sim 700$ nm. The high charge collection achieved from λ = 600 nm to 950 nm is remarkable for a QD film. We remark that our intercalated and bottom devices show low performance at $\lambda \sim 500$ nm, which can be due to degradation by device fabrication in air and the Gr transfers in aqueous solutions. Some reports show significant degradation of PbS-QD devices in the visible range after air exposure.[11,24,25] This can eventually be corrected by implementing the fabrication process in a glove box and using Gr dry transfers. Further confirmation of the superior performance of intercalated devices is shown in Fig. 3d, showing R as function of light intensity with a λ = 850 nm laser (dark current traces are shown in Fig. S5†). Over the power intensity range of 10^{-5} to 10^{1} mW cm^{-2}, the 1-micron thick device has a 2-orders of magnitude improvement in photoresponsivity over the 1-micron thick bottom device. The decrease in responsivity as light intensity (P_{inc}) increases reflects the $R \sim P_{inc}^{\beta-1}$ ($\beta < 1$) behavior of Gr/QD photodetectors,[19] observed in several QD photodetector reports.[12,15,19,21] This behavior is mainly due to lower lifetime as light intensity increases, reducing the photogain. The intercalated architecture also results in improved detectivity (D^*), reaching $D^* = 4.31 \times 10^{12}$ Jones (NEP = 2.35×10^{-14} W Hz$^{-1/2}$) for intercalated devices and $D^* = 1.1 \times 10^{11}$ Jones (NEP = 9.01×10^{-13} W Hz$^{-1/2}$) for bottom devices at 20 Hz (dark/noise levels shown in Fig. S5†).

Gr/QD intercalated devices can be easily fabricated and implemented on flexible substrates. CVD-grown single layer graphene and QDs were sequentially deposited on a polyethyl-

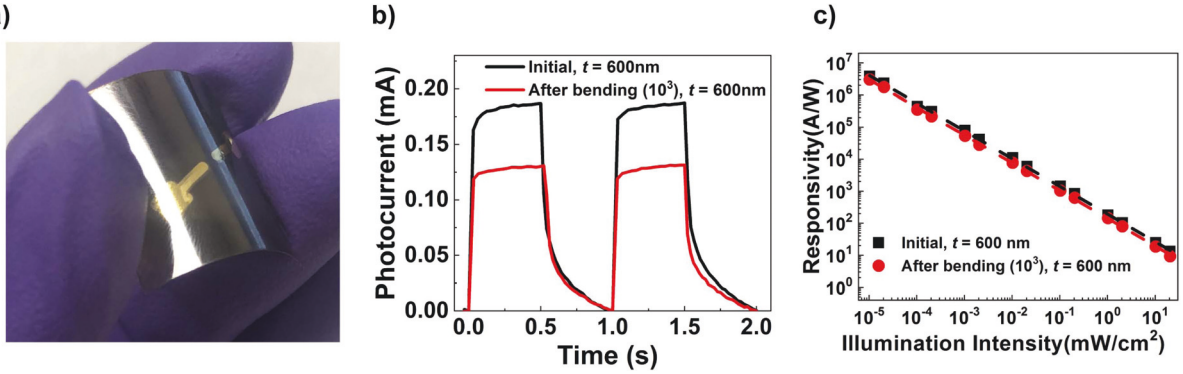

Fig. 4 Responsivity of intercalated device on flexible PET substrate. (a) Optical image of QDs and graphene intercalated device on PET substrate, QDs thickness t = 600 nm. (b) Light response of device in (a) before and after a bending test for 1000 times under 1 V bias, λ = 850 nm P_{inc} = 3.5 mW. (c) Responsivity of the flexible VIAs device as a function of incident light intensity characterized before and after bending test under 5 V bias, λ = 850 nm laser diode.

ene terephthalate (PET) substrate. Fig. 4a shows the optical image of the PET substrate with Gr/QD intercalated film. Fig. 4b and c show the light response of the flexible VIAs device (t = 600 nm) under 850 nm light irradiation before and after a bending test for 1000 times, showing up to 70% degradation in response after 1000 bending cycles. Therefore, intercalated devices can be easily applied onto flexible substrate for wearable sensing, imaging and other optoelectronic applications.

The 1 μm intercalated QD films herein presented achieve improved photodetection exhibiting high EQE ~ 70–90% across the λ = 600–950 nm range without the typical drop near λ ~ 700 nm observed in top/bottom QD photodetectors and photovoltaic cells. The intercalating graphene layers using VIAs allows efficient charge collection despite the total QDs film thickness, breaking the restriction that short diffusion length imposes on the thickness of QDs films. The intercalated configuration herein presented has a direct application to improve broadband spectrum detection towards the infrared using Gr/QD. Recently, the integration of Gr/QD with CMOS has shown the power of this hybrid technology for broad spectrum imaging.[26] In order to push Gr/QD/CMOS detection technology towards longer wavelengths with deeper penetration depths, thicker QD films can be required, in which case, intercalated films can be the perfect tool to improve photon capture keeping charge collection. Another exciting but more challenging path forward is to apply the intercalated architecture to photovoltaic cells intercalating QDs with n- and p-type intercalated layers, such as MoS_2 (n-type)[21,22] and Gr (p-type), allowing to separate both electrons and holes to obtain a photovoltaic cell. State-of-the-art solar cells (t ~ 250 nm) from leading groups in QDs typically show high EQE ~ 80% in the λ ~ 400–700 nm range, with strong decline to 50% in the λ ~ 700–1000 nm range. A recent device using a 2D-Matrix of QDs reported 600 nm thick devices but with overall power conversion limited to 12%.[9] Improving EQE to ~95% in the entire λ ~ 400–1000 nm range would help collecting almost the entire sunlight photon influx above the bandgap, potentially boosting the photovoltaic performance of QD solar cells from the current 10–15% range[6,8,27,28] towards 20%. 1-Micron thick QDs films with intercalated electrodes represent a potential path forward to achieve 20% efficiencies with QD solar cells.

4. Conclusion

In conclusion, we have presented a technology enables strong and uniform EQE in the λ = 600–950 nm range based on intercalated graphene collectors. The intercalated configuration herein presented has a direct application to improve broadband spectrum detection towards the infrared using Gr/QD. It also offers a potential path forward for intercalated photovoltaic devices by integrating QDs with n- and p-type layers to separate electrons and holes. Intercalated photovoltaic devices with 1 μm thick QD films could achieve high and uniform QE across the λ = 400–1000 nm range to boost QD photovoltaic conversion efficiencies towards 20%. The charge collection by graphene can also be affected by the QD ligands, therefore a study on the best ligands to improve charge transfer and stability between QD and Gr can lead to improved performance of this intercalated architecture. This intercalated technology is not restricted to QDs, it can also be expanded to improve the performance of optoelectronic devices using low-cost materials such as organic molecules, polymers, amorphous materials, or any other material that offers strong light absorption but has short diffusion length.

Conflicts of interest

There are no conflicts of interest to declare.

Acknowledgements

This work was supported by the National Science Foundation under Award No. 1710472. This work was performed in part at

the San Diego Nanotechnology Infrastructure (SDNI) of UCSD, NANO3, a member of the National Nanotechnology Coordinated Infrastructure, which is supported by the National Science Foundation (Grant ECCS-1542148). Seungbae Ahn is supported by the Kwanjeong Fellowship from the Kwanjeong Educational Foundation.

References

1 Z. S. Hosseini, H. A. Bafrani, A. Naseri and A. Z. Moshfegh, High-performance UV-Vis-NIR photodetectors based on plasmonic effect in Au nanoparticles/ZnO nanofibers, *Appl. Surf. Sci.*, 2019, **483**, 1110–1117.
2 Y. H. Zhou, H. N. An, C. Gao, Z. Q. Zheng and B. Wang, UV–Vis-NIR photodetector based on monolayer MoS_2, *Mater. Lett.*, 2019, **237**, 298–302.
3 J. M. Luther, *et al.*, 001-Schottky solar cells based on colloidal nanocrystal films, *Nano Lett.*, 2008, **8**, 3488–3492.
4 H. Lu, G. M. Carroll, N. R. Neale and M. C. Beard, Infrared Quantum Dots: Progress, Challenges, and Opportunities, *ACS Nano*, 2019, **13**, 939–953.
5 R. A. Taylor and K. Ramasamy, Colloidal quantum dots solar cells, *SPR Nanosci.*, 2017, **4**, 142–168.
6 C.-H. M. Chuang, P. R. Brown, V. Bulović and M. G. Bawendi, Improved performance and stability in quantum dot solar cells through band alignment engineering, *Nat. Mater.*, 2014, **13**, 796–801.
7 D. Zhitomirsky, O. Voznyy, S. Hoogland and E. H. Sargent, Measuring charge carrier diffusion in coupled colloidal quantum dot solids, *ACS Nano*, 2013, **7**, 5282–5290.
8 X. Lan, *et al.*, 10.6% Certified Colloidal Quantum Dot Solar Cells Via Solvent-Polarity-Engineered Halide Passivation, *Nano Lett.*, 2016, **16**, 4630–4634.
9 J. Xu, *et al.*, 2D matrix engineering for homogeneous quantum dot coupling in photovoltaic solids, *Nat. Nanotechnol.*, 2018, **13**, 456–462.
10 X. Lan, *et al.*, Passivation Using Molecular Halides Increases Quantum Dot Solar Cell Performance, *Adv. Mater.*, 2016, **28**, 299–304.
11 Z. Ning, *et al.*, Air-stable n-type colloidal quantum dot solids, *Nat. Mater.*, 2014, **13**, 822–828.
12 G. Konstantatos, *et al.*, Hybrid graphene–quantum dot phototransistors with ultrahigh gain, *Nat. Nanotechnol.*, 2012, **7**, 363–368.
13 D. Kufer, I. Nikitskiy, T. Lasanta, G. Navickaite, F. H. L. Koppens and G. Konstantatos, Hybrid 2D-0D MoS_2-PbS quantum dot photodetectors, *Adv. Mater.*, 2015, **27**(1), 176–180.
14 I. Nikitskiy, *et al.*, Integrating an electrically active colloidal quantum dot photodiode with a graphene phototransistor, *Nat. Commun.*, 2016, **7**, 11954.
15 W. Chen, J. Castro, S. Ahn, X. Li and O. Vazquez-Mena, Improved Charge Extraction Beyond Diffusion Length by Layer-by-Layer Multistacking Intercalation of Graphene Layers inside Quantum Dots Films, *Adv. Mater.*, 2019, **31**, 1–6.
16 X. Lan, S. Masala and E. H. Sargent, Charge-extraction strategies for colloidal quantum dot photovoltaics, *Nat. Mater.*, 2014, **13**, 233–240.
17 J. Tang and E. H. Sargent, Infrared colloidal quantum dots for photovoltaics: Fundamentals and recent progress, *Adv. Mater.*, 2011, **23**, 12–29.
18 E. H. Sargent, Colloidal quantum dot solar cells, *Nat. Photonics*, 2012, **6**, 133–135.
19 Z. Sun, *et al.*, Infrared photodetectors based on CVD-grown graphene and PbS quantum dots with ultrahigh responsivity, *Adv. Mater.*, 2012, **24**, 5878–5883.
20 W. Chen, S. Ahn, C. Rangel and O. Vazquez-Mena, Implementation of Metallic Vertical Interconnect Access in Hybrid Intercalated Graphene/Quantum Dot Photodetector for Improved Charge Collection, *Front. Mater.*, 2019, **6**, 1–7.
21 D. Kufer, *et al.*, Hybrid 2D-0D MoS 2-PbS Quantum Dot Photodetectors, *Adv. Mater.*, 2014, DOI: 10.1002/adma.201402471.
22 D. Kufer, T. Lasanta, M. Bernechea, F. H. L. Koppens and G. Konstantatos, Interface Engineering in Hybrid Quantum Dot-2D Phototransistors, *ACS Photonics*, 2016, **3**, 1324–1330.
23 D. Kufer and G. Konstantatos, Photo-FETs: Phototransistors Enabled by 2D and 0D Nanomaterials, *ACS Photonics*, 2016, **3**, 2197–2210.
24 G. Zhai, A. Bezryadina, A. J. Breeze, D. Zhang, G. B. Alers and S. A. Carter, Air stability of TiO 2/PbS colloidal nanoparticle solar cells and its impact on power efficiency, *Appl. Phys. Lett.*, 2011, **99**(6), 063512.
25 W. Gao, *et al.*, Towards understanding the initial performance improvement of PbS quantum dot solar cells upon short-term air exposure, *RSC Adv.*, 2018, **8**(27), 15149–15157.
26 S. Goossens, *et al.*, Broadband image sensor array based on graphene-CMOS integration, *Nat. Photonics*, 2017, **11**, 366–371.
27 E. M. Sanehira, *et al.*, Enhanced mobility CsPbI 3 quantum dot arrays for record-efficiency, high-voltage photovoltaic cells, *Sci. Adv.*, 2017, **3**, eaao4204.
28 A. Stavrinadis, S. Pradhan, P. Papagiorgis, G. Itskos and G. Konstantatos, Suppressing Deep Traps in PbS Colloidal Quantum Dots via Facile Iodide Substitutional Doping for Solar Cells with Efficiency >10%, *ACS Energy Lett.*, 2017, **2**, 739–744.
29 B. Hou, *et al.*, Highly Monodispersed PbS Quantum Dots for Outstanding Cascaded-Junction Solar Cells, *ACS Energy Lett.*, 2016, **1**, 834–839.
30 R. X. He, *et al.*, Solution-gated graphene field effect transistors integrated in microfluidic systems and used for flow velocity detection, *Nano Lett.*, 2012, **12**, 1404–1409.
31 T. Mueller, F. Xia and P. Avouris, Graphene photodetectors for high-speed optical communications, *Nat. Photonics*, 2010, **4**, 297–301.